

Physicochemical Properties and Catalytic Performances of Nanostructured V_2O_5 over TiO_2 and $\gamma-Al_2O_3$ for Oxidative Dehydrogenation of Propane

M. Kazemeini,^{a,b,*} M. Nikkhah,^a M. Fattahi,^c and L. Vafajoo^b

^aDepartment of Chemical and Petroleum Engineering, Sharif University of Technology, Azadi Avenue, P.O. Box 11365-9465, Tehran, Iran

^bChemical and Environmental Engineering Group, College of Engineering, Ahang Blvd., Tehran, Iran

^cDepartment of Chemical Engineering, Abadan Faculty of Petroleum Engineering, Petroleum University of Technology, Abadan, Iran

doi: 10.15255/CABEQ.2014.2049

Original scientific paper

Received: May 21, 2014

Accepted: December 26, 2015

Samples of V_2O_5 catalysts supported on nanostructures of TiO_2 and $\gamma-Al_2O_3$ were synthesized through the hydrothermal method and used for the oxidative dehydrogenation of propane (ODHP) to propylene. The TiO_2 support was utilized in both commercial microstructure and synthesized nanostructure forms. Moreover, the $\gamma-Al_2O_3$ support was synthesized through chemical and precipitation methods. The vanadium catalyst was then deposited onto the hybrid of the TiO_2 and $\gamma-Al_2O_3$ materials. All prepared catalysts were characterized through the BET, FESEM, FTIR, XRD and TPR techniques. Performances of the synthesized catalysts were subsequently examined in a fixed-bed reactor. The main products were propylene, ethylene and CO_x . The prepared catalysts over TiO_2 and $\gamma-Al_2O_3$ were evaluated under reactor test conditions of 500 °C, feed of C_3H_8 /air with molar ratio of 0.6, and total feed flow rate of 90 mL min⁻¹. These resulted in optimum values of 35.53 and 23.88 % for the propylene selectivity and propane conversion, respectively 6 h after the start of the reaction. The comparison of performances made between the synthesized materials and those available in the open literature for the ODHP reaction was indeed satisfactory.

Key words:

oxidative dehydrogenation, nanostructure, V_2O_5 , hydrothermal method, TiO_2/Al_2O_3

Introduction

Propylene is an important raw material and extensively used in the petrochemical industry. There has been a continuously growing demand for propylene in recent years around the world^{1–3}. The majority of propylene is produced as a byproduct from processes such as steam cracking of naphtha and fluid catalytic cracking (FCC)^{4,5}. Additional sources of propylene included dehydrogenation of propane, olefin metathesis, and natural gas-based processes. The strong demand on propylene has stimulated studies focused on development of new methods of propylene production from alternative substrates and improvement of the propylene yield from the existing processes⁶. Yet, an additional source of propylene was dehydrogenation of propane. This indeed was of considerable industrial importance since it represented a route economically upgrading low-cost saturated propane into the more expensive propylene⁷. Even though dehydrogenation of propane was more selective than the established pro-

cesses, its yield of propylene was strongly influenced by the process conditions, including temperature, feed, and contact time. Byproducts obviously increased the separation costs and coke formation enforcing frequent catalyst regeneration⁸. The addition of O_2 in terms of N_2O to the reaction mixture allowed performing exothermic oxidative dehydrogenations (ODHs). The process had no thermodynamic limitations and prevented the growth of carbonaceous deposits over the catalyst⁹. The development of active and selective catalytic materials for the oxidative dehydrogenation of light alkanes to their corresponding alkenes has been the focal study point of many academic and industrial research groups^{10–19} through which, usually, the Mars–van Krevelen mechanism was assumed for the ODHP reaction. To begin with, the propane reacted with the lattice oxygen of the oxidic catalyst, such as V_2O_5 through which the first and then second hydrogen were abstracted from the hydrocarbon molecule. This formed two OH^- groups on the surface of the catalyst coupled to produce water and desorb from the solid surface. In this venue, the propylene yield of 10 % was usually considered

*Corresponding author: e-mail: kazemini@sharif.edu, kazemini@azad.ac.ir; tel.: +98 6616 5425; fax: +98 6602 2853

very satisfactory (e.g., for 20 % propane conversion with 50 % propylene selectivity)²⁰. The selection or development of an appropriate catalyst for each of these reactions under low temperature conditions and in the presence of oxygen might have promoted the light alkanes activation towards formation of highly selective alkenes. The achievement of this was indeed a challenging task. Different catalytic systems were reported to be active and selective in the ODHP process. Examples of these included supported vanadia catalysts, metal tungstates, metal molybdates, metal phosphates, Keggin-polyoxo-tungstates and supported transition metal oxides²⁰. Transition metal oxides were commonly used for the oxidation of hydrocarbons^{21–23}. Amongst the catalysts developed, those that contained vanadia demonstrated higher activity and selectivity towards the ODHP^{8,9,24–26}. Moreover, supported vanadium oxides attracted much attention due to their higher performance, better thermal stability, and larger surface area^{24,27,28}. Furthermore, vanadia was also commonly used on metal oxide supports, including TiO₂, SiO₂ and Al₂O₃ for such purposes²². The catalytic performance of vanadia-supported catalysts in the ODH of alkanes depended on the nature of the support, the preparation procedure, and the vanadia loading²¹. Acidic and basic natures as well as the redox characters revealed to be the most important factors affecting the performance of the selective oxidation catalysts. Corma *et al.* found that, in the ODHP, the most selective catalysts were obtained with V supported upon basic rather than acidic metal oxides. Arena *et al.* reported that the reactivity of V upon various supports was highest when deposited on amphoteric oxides (e.g. TiO₂)²⁹. Doping of V₂O₅/TiO₂ catalysts with alkali metals was investigated by Aranda *et al.*, who provided interesting results making a connection between the catalyst performance in the ODH of propane and its surface characteristics³⁰.

This research investigates the catalytic activity of the V₂O₅ catalyst decorated onto TiO₂ and γ -Al₂O₃ by the hydrothermal method utilized in the ODHP reaction. The synthesized catalysts were characterized by the BET, XRD, FTIR, H₂-TPR and FESEM techniques. Moreover, the evaluation of the as-synthesized catalyst along with the precursor effects on the template nanostructure preparation (*i.e.* Al₂O₃ prepared through ammonium hydrocarbonate and sodium hydroxide) were studied in a conventional fixed-bed reactor at 500 °C, feed of C₃H₈/air with molar ratio of 0.6, and total feed flow rate of 90 mL min⁻¹. The novelty of this study was to provide a simple yet effective catalyst synthesis route towards achieving a better performance of the ODHP reaction.

Experimental

Catalyst preparation

Synthesis of the TiO₂ nanorods by the hydrothermal method

A commercial TiO₂ powder (Merck) was used as a starting material. A total of 2 g of TiO₂ powder and 25 mL of 10 M NaOH aqueous solution were put into a Teflon-lined stainless steel autoclave. This was heated and stirred at 150 °C for 48 hours. Thereupon, it was naturally quenched to room temperature. The obtained precipitate was then washed several times with distilled water, filtered, and transferred into a 500 mL of 0.1 M HCl aqueous solution and stirred for 24 hours. This HCl treatment was repeated three times in order to remove residual Na⁺. The obtained precipitate was washed with distilled water for several times, and dried at 80 °C.

Synthesis of the Al₂O₃ nanorods by the precipitation method

A 0.1 M solution of aluminum nitrate (Al(NO₃)₃ · 9H₂O, Merck) and 0.4 M solution of ammonium hydrogen carbonate ((NH₄)HCO₃, Merck) were prepared. The aluminum nitrate solution was added drop-wise to a precipitation vessel containing distilled water under vigorous mixing at 70 °C. The ammonium hydrogen carbonate solution was then added to the precipitation vessel at an adjusted rate assuring a nearly constant pH for the solution at approximate value of 8.0 during the experiment. After precipitation was complete, the dried precipitates were digested for 3 h at 70 °C under mild mixing conditions. The precipitates were then filtered and washed with ethanol and acetone (composition of 50–50 % v/v), respectively, to remove residual sodium contamination. The resulting precipitates were dried at room temperature and calcinated in air at 550 °C for 5 hours. The precipitation experiment was repeated with sodium hydroxide (NaOH) as the precipitating agent, utilizing the same conditions outlined above for the ammonium hydrogen carbonate.

Synthesis of V₂O₅ over a hybrid of TiO₂ and Al₂O₃ by the hydrothermal method

Titanium dioxide in two types, including synthesized nanostructure and commercial microstructure, as well as prepared alumina in two types designated as Al₂O₃-type1 (using ammonium hydrogen carbonate as the precipitating agent) and γ -Al₂O₃-type2 (using sodium hydroxide as the precipitating agent) were prepared by the precipitation method in a Al:Ti molar ratio of 1:1 dissolved in 200 mL of ethanol. The solution temperature was raised to 80 °C

under vigorous stirring for 90 minutes. This solution and 20 mL of water were added to a Teflon-lined autoclave with a stainless steel shell kept at 200 °C for 36 hours. The resulting precipitate was neutralized by filtering and washing. This precipitate was then washed with a solution of ethanol and n-hexane (composition of 50–50 % v/v), dried at 80 °C for 12 h to ultimately obtain titanium dioxide over Al_2O_3 . The samples were subsequently calcined at 400 °C for 2 h under nitrogen atmosphere.

The vanadium pentoxide (V_2O_5) and $\text{TiO}_2/\gamma\text{-Al}_2\text{O}_3$ in a molar ratio of 1:1 were then dissolved in 50 mL of ethanol and 50 mL of distilled-deionized water. The solution temperature was raised to 80 °C under vigorous stirring for 60 minutes. This solution was then added to a Teflon-lined autoclave with a stainless steel shell kept at 200 °C for 24 hours. The resulting precipitate was neutralized by filtering and washing. This material was then washed with a solution of ethanol and n-hexane (composition of 50–50 % v/v), dried at 80 °C for 12 h to ultimately result in V_2O_5 over $\text{TiO}_2/\gamma\text{-Al}_2\text{O}_3$ catalyst. The samples were subsequently calcined at 400 °C for 2 h under air atmosphere.

The resulting catalysts prepared by the hydrothermal method are listed in Table 1. Their performance tests were carried out in a conventional tubular fixed-bed quartz reactor.

Table 1 – Types of the synthesized catalysts in this research

Catalyst	Type
Cat1	Nano TiO_2
Cat2	$\text{V}/\text{TiO}_2\text{-Al}_2\text{O}_3\text{1}$
Cat3	$\text{V}/\text{Nano TiO}_2\text{-Al}_2\text{O}_3\text{1}$
Cat4	$\text{V}/\text{TiO}_2\text{-Al}_2\text{O}_3\text{2}$
Cat5	$\text{V}/\text{Nano TiO}_2\text{-Al}_2\text{O}_3\text{2}$

Catalyst characterization techniques

Powder X-ray diffraction (XRD) analysis was performed using a TOE Analytical X-ray diffractometer with Cu-K_α radiation (40 kV, 30 mA). The spectra were measured with a step size of 0.08° over a 2θ range of $3^\circ\text{--}120^\circ$. The range chosen was wide enough to cover all significant diffraction peaks aimed at the crystal structures to be examined. Mean crystallite size of the catalysts determined by the Scherrer formula confirmed the one obtained using the FESEM method.

The pore size, textural properties, and specific surface area of the catalysts were measured by nitrogen adsorption-desorption at -196°C using the

ASAP apparatus, model 2010 (Belsorp mini II manufactured by BEL-Japan). The samples were first degassed under vacuum at 200 °C for 12 hours. The BET and BJH methods were utilized for measuring the specific surface area, total pore volume, and average pore diameter.

UV-visible spectroscopy was performed by the AvaSpec-2048 equipped with a diffusion reflectance accessory.

The TPR experiments were carried out in a BEL-CAT (type A, Japan) instrument coupled with a gas flow controller. The catalysts were heated in a 6.52 % (v/v) H_2 in Ar from room temperature up to 800 °C at a heating rate of 5°C min^{-1} , and flow rate of 150 mL min^{-1} . Subsequently, the FTIR analyses were performed and recorded on an ABB Bomem MB-100 spectrophotometer. These spectra were obtained from KBr pellets taken from 4000 to 400 cm^{-1} with a resolution of 4 cm^{-1} .

Field emission scanning electron microscope (FESEM) images were obtained with a Hitachi S-4160 device. Gold was used as a conductive material for sample coating.

Experimental set-up

Catalyst performance tests were carried out in a conventional tubular fixed-bed quartz reactor. The schematics of the experimental setup utilized in this research is shown in Figure 1. The reactor was

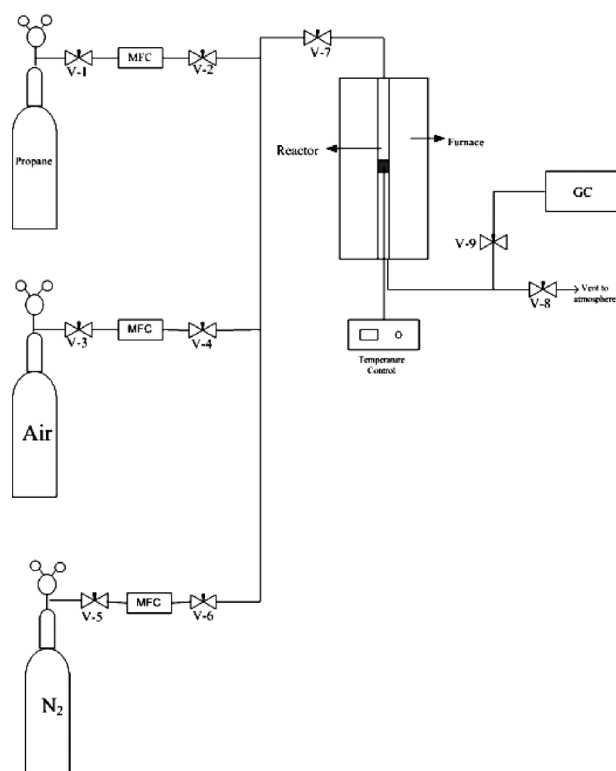


Fig. 1 – Schematic diagram of the experimental apparatus utilized in this study

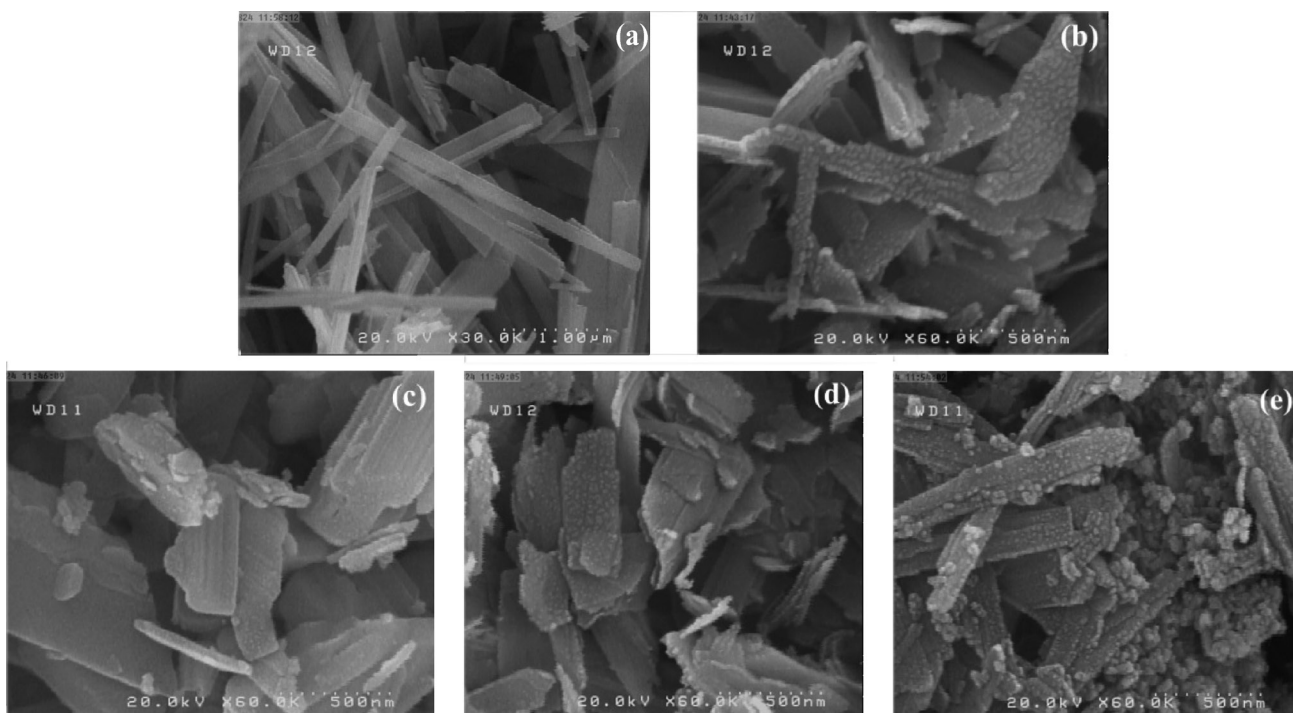


Fig. 2 – FESEM micrographs of the prepared materials: (a) Cat1, (b) Cat2, (c) Cat3, (d) Cat4 and (e) Cat5

10 mm in diameter and 70 cm long. It was placed in an electrical furnace equipped with a temperature controller to maintain the reactor temperature to within ± 1 °C of the desired set point using thermocouples placed both on the inside and on the external surface of the reactor. The catalyst loading was 0.5 g mixed with 0.5 g quartz beads for all ODHP experiments. The nitrogen, air, and propane utilized were of purity above 99.9 % purity. The reactor was purged at room temperature with nitrogen for 2 hours. The reactor temperature was then increased to the desired value with a temperature ramp of 5 °C min^{-1} . The reaction temperature was set to be in the range of 400–500 °C. This choice was a compromise between several factors, including energy saving in the petrochemical processes, as well as the inactivity of the catalysts below 300 °C.² Moreover, these operating conditions were selected based upon the optimization considerations in a recent study of this research group².

Air and propane flow rates were controlled by mass flow controllers. The exit gases were analyzed for light hydrocarbons, CO, and CO₂ using an on-line Agilent gas chromatograph equipped with both TCD and FID detectors. In a typical experiment, product samples were determined after the start of the run when stationary conditions are achieved. In other words, these samples were detected hourly after the run had started. Moreover, the propane conversion, product selectivity, and propylene yield were defined as follows:

$$\text{Propane conversion (\%)} = \frac{\sum_i \left(\frac{n_i}{3}\right) [F_i]_{out} - [F_{C_3H_8}]_{out}}{\sum_i \left(\frac{n_i}{3}\right) [F_i]_{out}} \cdot 100$$

$$\text{Selectivity for component } i \text{ (\%)} = \frac{\left(\frac{n_i}{3}\right) [F_i]_{out}}{\sum_i \left(\frac{n_i}{3}\right) [F_i]_{out} - [F_{C_3H_8}]_{out}} \cdot 100$$

$$\text{Propylene yield (\%)} = \frac{\text{Propane conversion} \cdot \text{Selectivity of propylene}}{100}$$

where i included all the components containing carbon atoms in the exit gas stream, n_i the number of carbon atoms of component i and F_i was its outlet molar flow rate.

Catalyst characterization results

Figures 2a–2e demonstrate the FESEM micrographs for the prepared catalysts in this work. The regular bar-like morphology in Figure 2(a) illustrate the nanostructure of the TiO₂ alone, while the irregular sheets in Figures 2b–2e indicate the presence of Al₂O₃, possessing lighter color than TiO₂, in the catalyst structure. The prominences on the surface of

the catalyst revealed the growth of the V_2O_5 species. The width of these sheets was about 80–170 nm and their length reached up to micron scale. The synthesized material was made of a homogenous phase with particles almost uniformly sized displaying nanorod morphology on which the vanadium particles sprouted. This might have led to a possible enhancement towards: i) assisting of the dispersion of vanadium components in the solution, and ii) helping the media for vanadium growth. Moreover, in the case of the pristine V_2O_5 nanostructure, the active species were vulnerable to clustering in sizes down to hundreds of nanometers; however, their greater dispersion on the surface of the supports might have led to larger sizes, thus alleviating this problem.

Figure 3 shows the FTIR spectra of catalysts prepared in this research. The broad IR spectra indicates strong absorptions at 450 to 500 cm^{-1} relating to symmetric and asymmetric stretching catalyst vibrations of V-O-V, and at 750 to 800 cm^{-1} assigned to the stretching of the short Ti-O bonds. The spectrum of the as-prepared catalysts showed the Al-O stretching bonds in the range of 1600 to 1700 cm^{-1} . Besides, the spectrum of the structured material produced by hydrothermal treatment, washed many times, and dried at 80 °C, contained an absorption band in the range 3200–3600 cm^{-1} . This was a characteristic of asymmetric and symmetric $\nu(OH)$ stretching vibrations after absorbed water. Moreover, a weak, broad band observed in the range 1000–1500 cm^{-1} was attributed to the $\delta(HOH)$ bending vibrations in water molecules adsorbed on the surface of the material and/or located in the micro- and macropores³¹. In addition, the spectrum contained strong absorption bands centered at around 650 cm^{-1} arising from the $\nu(Ti-O)$ stretching modes of the TiO_6 titanium–oxygen octahedron^{31,32}. In catalysts containing nano- TiO_2 like the one in this study, the results revealed the existence of individual bands at 1400 to 1300 cm^{-1} , due to the $\delta(-Ti-O(H)-Ti)$ and $\delta(OH)$ in-plane bending modes,

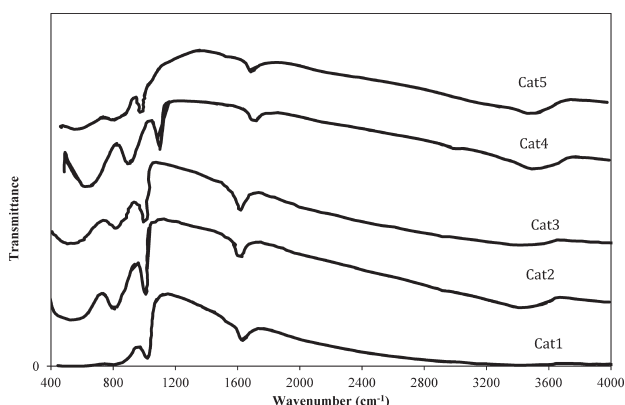


Fig. 3 – FTIR spectra of the synthesized catalysts in this work

respectively⁹. Moreover, a weak band at 1100 cm^{-1} rose from the $\delta(Ti-O-H)$ bending mode of surface groups¹⁰. Instead of the absorption band of the $\nu(-Ti-O)$ stretching mode, there was a broad band at 750 cm^{-1} seemingly indicating severe distortion of the titanium–oxygen octahedron in the structures of the forming compounds^{31,32}.

In addition, the spectra of the samples shown in Figure 3 revealed a band at around 2000 cm^{-1} which was assigned to the V=O bond overtone vibration³³. The intensity of the overtone band might be predicted to be continuously increased with an enhanced vanadia loading. The Ti–Al support was revealed by the low IR bands at 3000, 3500 and 3800 cm^{-1} . The corresponding bands were assigned to basic, neutral, and acidic OH⁻ groups of alumina³⁴. The IR band at 3700 cm^{-1} was also assigned to the isolated hydroxyl group vibration of titania, and the band at 3800 cm^{-1} assigned to the bridged hydroxyl group vibration of titania³⁴. The low intensity of bands at above 3500 cm^{-1} was titrated even at the lowest vanadia loading. The presence and gradual disappearance of the titania and alumina hydroxyls with vanadia loading suggested that titania and alumina were present on the surface of the mixed oxide support synthesized. It is noteworthy that, in the current study, this was coordinated with the surface vanadia species. Furthermore, the preferential titration of the titania hydroxyl versus the alumina hydroxyl group was not evident. In addition, the Cat1 behavior shown in Figure 3 indicated two peaks at wavenumbers of 430 and 500 cm^{-1} related to symmetric and asymmetric Ti-O bonds.

The X-ray diffraction (XRD) patterns for vanadium catalysts over TiO_2 and alumina synthesized by the hydrothermal method are presented in Figure 4. The diffraction patterns for all catalysts expect that of Cat1, displayed 10 distinct reflections, four of which were located at $2\theta = 15.4^\circ \pm 0.1$, $20.4^\circ \pm 1$, $22.1^\circ \pm 1$ and $31.4^\circ \pm 1$ assigned to V_2O_5 . In addition, the distinct reflection located at $2\theta = 26.4^\circ \pm 1$ was assigned to A- TiO_2 (*i.e.* the Anatase phase), while that located at $2\theta = 34.5^\circ \pm 1$ corresponded to the R- TiO_2 (*i.e.* the Rutile phase). Finally, the distinct reflections located at $2\theta = 32.5^\circ \pm 1$, $47.6^\circ \pm 1$, $50.6^\circ \pm 1$ and $60.3^\circ \pm 1$ were assigned to γ -alumina. In Cat1 material's behavior, the four distinguished reflections, located at $2\theta = 12.1^\circ \pm 1$ and $23.7^\circ \pm 1$ were assigned to the A- TiO_2 and at $2\theta = 29.1^\circ \pm 1$ and $47.7^\circ \pm 1$ corresponded to the R- TiO_2 .

All samples exhibited diffraction peaks characteristic of the materials and supports utilized. The diffraction lines corresponding to V-containing compounds were detected in the vanadium samples, indicating that the vanadia species were rather highly dispersed on the support surface. Highly dispersive vanadia might normally show no diffraction

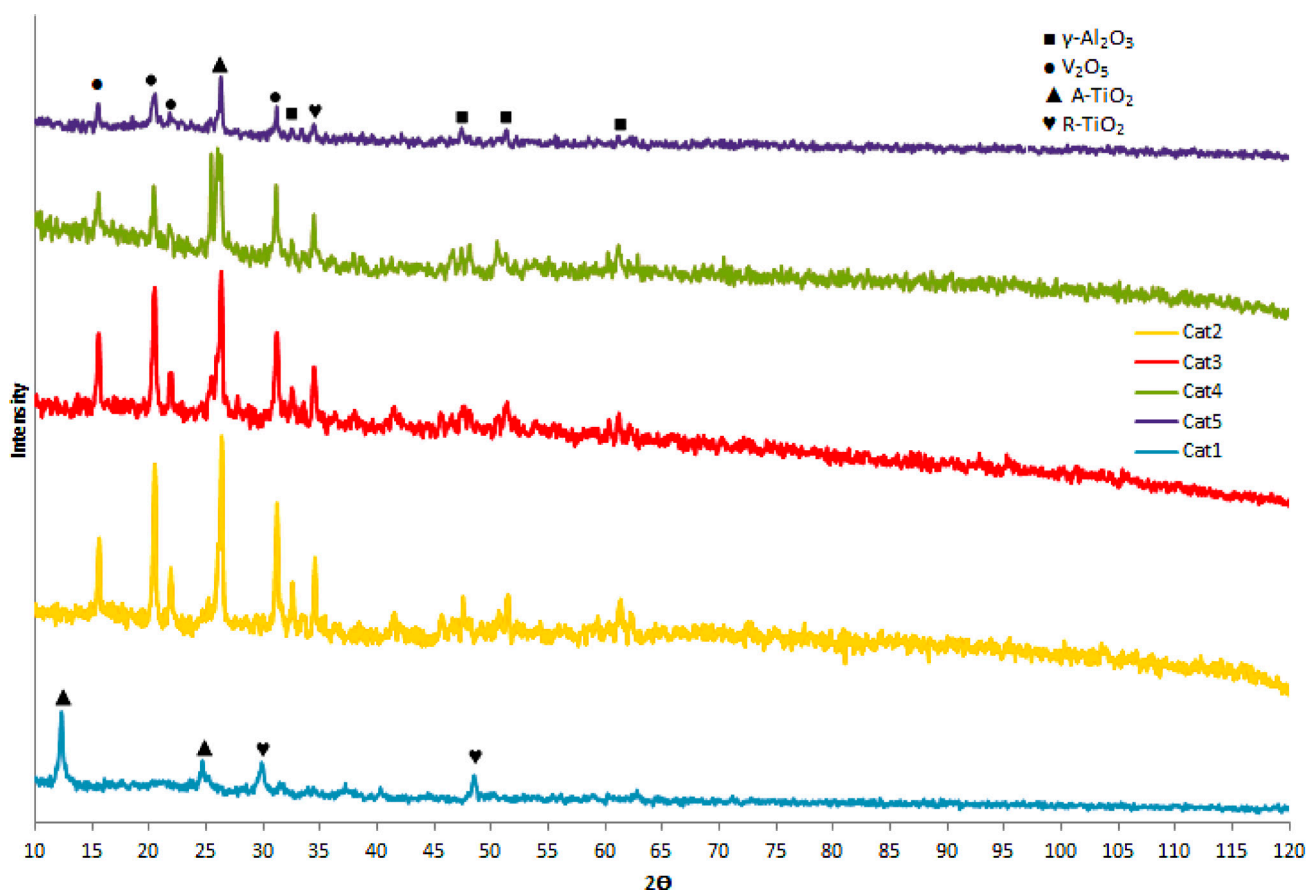


Fig. 4 – XRD pattern of the synthesized catalysts in this research

peaks or very broad XRD features. Moreover, the obvious peaks showed no diffraction peaks that re-confirmed the good dispersion of the vanadia compounds. The same behavior was also observed with the vanadia on titania catalysts. However, with the alumina-supported V catalyst, it was clear that, even though the theoretical coverage was almost equal to that of a monolayer, V_2O_5 crystallites were formed and detected in the XRD pattern of the sample. For catalysts containing the V-Ti-Al, the rutile and anatase phases were observed. Moreover, an additional peak around $2\theta = 22^\circ$ for crystalline V_2O_5 appeared³⁵. It seemed that, at the aforementioned calcination temperature, a bulk of the V_2O_5 was formed in the samples. From the previous discussions, it was also evident that the anatase to rutile phase transformation occurred in the vanadia-based samples. The lower anatase to rutile transformation temperature observed in the high vanadia containing samples is suggested to be due to: (i) the high mobility of V in the structure, (ii) incorporation of V in the titania anatase structure, and (iii) introduction of distortions into the respective structures^{36,37}.

The reduction behavior of the catalysts investigated by the H_2 -TPR technique and the results for the nanomaterials prepared are presented in Figure 5. In the TPR curve for the Cat3 material, three

distinguishable peaks appeared at about 678, 690 and 758 °C. On the other hand, for the Cat5 species, three relatively sharp and distinguishable peaks appeared at about 639, 696, and 796 °C, while for the Cat1 catalyst in Figure 5(b) one peak appeared at about 705 °C corresponding to the residual catalyst impurities in the sample. As these profiles revealed, a distinct reduction peak at the 600–800 °C region was displayed. The peak observed at the 600–700 °C region was due to the reduction of surface vanadia species shifting to higher temperatures as vanadia loading enhanced and its dispersion soared. In comparison to previous investigations, the reduction peaks for V_2O_5/TiO_2 (1–6 wt %) and V_2O_5/Al_2O_3 (7.5–17.5 wt %) catalysts were observed at 412–452 and 477–487 °C, respectively^{38,39}. It is well established that highly dispersed supported vanadia normally appears at about 400–500 °C, while crystalline V_2O_5 showed three peaks at higher temperatures. It is likely that the TPR profiles originated from large clusters of crystalline vanadia. These contrasting results attributed to different vanadia species loadings implemented in this study also led to better catalyst performance. Analysis of the reduction profiles of the V-Ti-Al samples further suggested that the surface vanadia species coordinated with titania and alumina of the mixed oxide support.

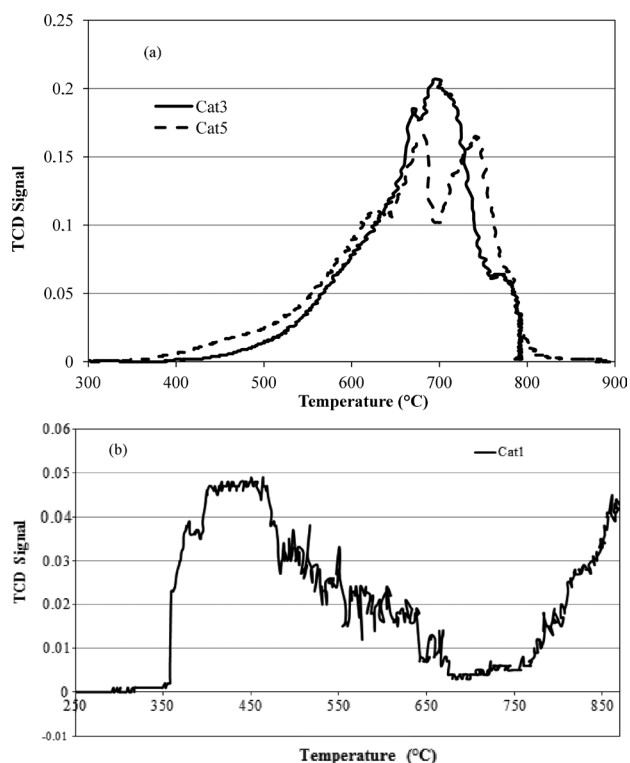


Fig. 5 – H_2 -TPR results for the (a): Cat3 and Cat5 materials and (b): Cat1 species

Porosimetry analyses of the synthesized catalysts are presented in Figure 6 for the two better nanomaterials prepared, namely Cat3 and Cat5 species. Figure 6(a) indicated that, nitrogen sorption isotherms of V_2O_5 over TiO_2 and Al_2O_3 were similar in shape. Both catalysts displayed the well-known type IV isotherm characteristic of materials with mesoporosity and a high energy of adsorption. Figure 6(b) illustrated the BJH pore size distribution of these catalysts. It was revealed that the Cat5 material had a wider pore size distribution than that of the Cat1 catalyst. The Cat1 had a surface area of $15.69 \text{ m}^2 \text{ g}^{-1}$ and an average pore diameter of 12.6 nm, while the Cat5 possessed a larger surface area of $38.4 \text{ m}^2 \text{ g}^{-1}$, and a larger average pore diameter of 18.4 nm. Nonetheless, the morphology of the Cat5 was generally less uniform in comparison with that of the Cat1 sample (see the FESEM micrographs).

Catalytic performance

For a better understanding of the prepared materials' behavior towards catalyzing the undertaken reaction, a comparative catalytic performance study was conducted under operating conditions of $500 \text{ }^\circ\text{C}$ and a total feed flow rate of 90 mL min^{-1} , utilizing a feed with C_3H_8 to air molar ratio of 0.6. This choice of conditions was rationalized earlier. The GC analyses of the product gases indicated that,

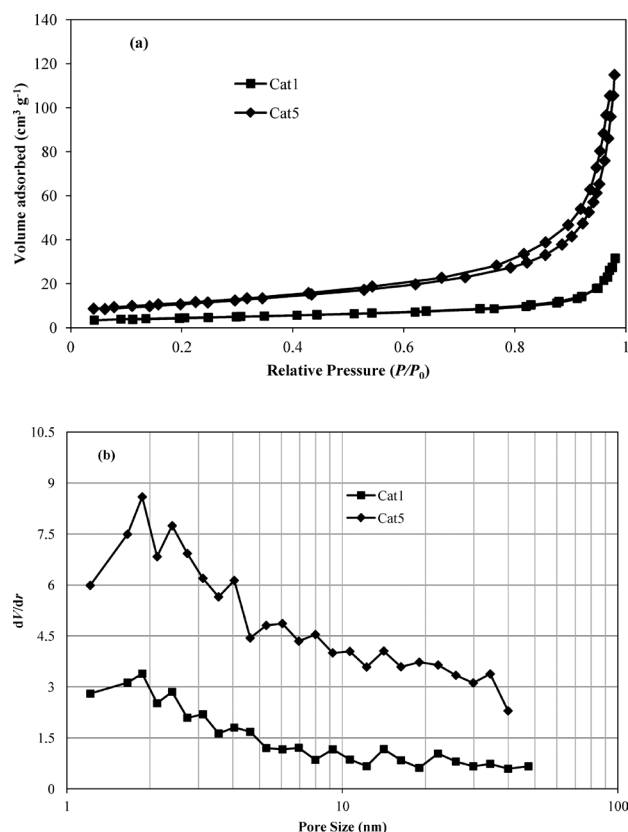


Fig. 6 – (a) Nitrogen sorption isotherms and (b) pore-size distributions for Cat1 and Cat5 samples

along with the unreacted propane, the main reaction products were propylene, ethylene, CO_2 and CO (together accounting for more than 99.5 % of the products), while no organic oxygenates were detected. These analyses of the products were performed hourly for a duration of 6 hours beginning from the start-of-run. Figure 7 presents propane conversions with different catalysts at the end of this time. Dissociative conversion of propane and propylene into ethylene and CO_x was revealed under the aforementioned reaction conditions. It was concluded that the CO_2 formation during the ODHP reaction had main-

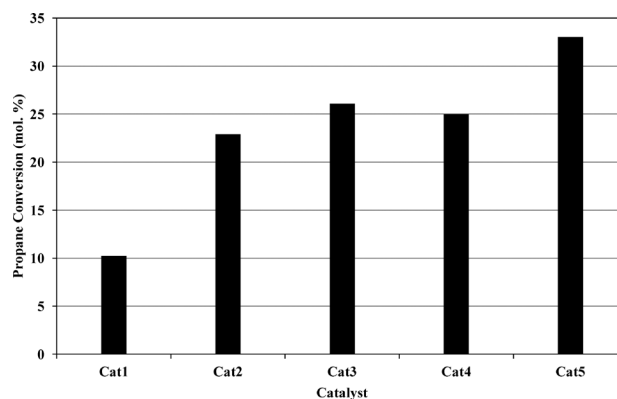


Fig. 7 – Propane conversions at $500 \text{ }^\circ\text{C}$, $C_3H_8/\text{air} = 0.6$ and feed flow rate of 90 mL min^{-1} for different catalysts investigated in this research

Table 2 – Values of propane conversion and product selectivities over different catalysts prepared in this work at $T = 500\text{ }^{\circ}\text{C}$, $C_3H_8/air = 0.6$, and total feed flow rate of 90 mL min^{-1}

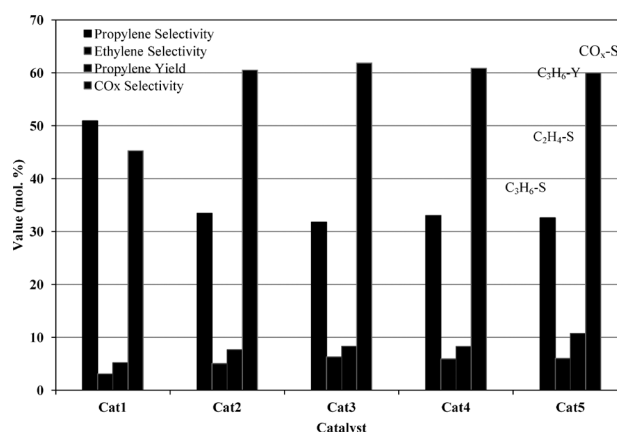
Catalyst	Propane conversion (%)	Propylene selectivity (%)	Ethylene selectivity (%)	CO _x selectivity (%)	Propylene yield (%)
Cat1	10.24	50.89	3.13	45.27	5.21
Cat2	22.92	33.44	5.04	60.51	7.66
Cat3	26.07	31.77	6.30	61.84	8.28
Cat4	24.98	31.02	5.92	60.87	7.75
Cat5	33.01	32.61	6.03	59.98	10.76

ly originated from oxidation of the hydrocarbon feedstock. Both propane conversion and propylene selectivity were shown to be sensitive to the support structure as well as any impurity or inactive species existing on the surface which might have acted as a site diluent increasing the selectivity toward dehydrogenation. It is noteworthy to mention that, based upon the previously published work of this research team², when utilizing the prepared catalysts, the oxidation reactions were more significant at lower temperatures while their oxy-cracking counterparts were more pronounced at elevated thermal conditions. Moreover, the catalysts prepared by the nano-TiO₂ had higher propylene yields in comparison with those prepared by the commercial TiO₂. Combustion of propane and propylene to form CO_x and its reforming to ethylene and CO_x were indeed important side reactions. Figure 8 indicates that the catalysts based upon Al₂O₃-2 prepared by both the nano- and industrial-TiO₂ demonstrated the lowest CO_x selectivities as well as the highest ratio of ethylene to CO_x selectivities in comparison with other synthesized catalysts in this research.

The mean values of the propane conversions and product selectivities during a 6-hour run over the aforementioned catalysts (e.g.; Cat1, Cat2, Cat3, Cat4, and Cat5) are summarized in Table 2. It was demonstrated that the catalysts prepared by commercial TiO₂ had much lower propylene yields and propane conversions in comparison with catalysts prepared utilizing the synthesized nano-TiO₂. Amongst all catalysts, the Cat5 material was recognized as the most effective catalyst for the ODHP reaction with mean values of 32.61 and 33.01 % for propylene selectivity and propane conversion, respectively.

It is noteworthy that, since in general, the production of CO_x led to lowering of the products' selectivities, the hydrothermal method might have helped to enhance the production of the active sites on the synthesized catalyst. This conclusion was drawn due to such prepared material demonstrating reversal of the aforementioned selectivity trend.

Ultimately, a comparison of reactor performance results between the best-obtained catalyst for the ODHP reaction in this work (i.e. Cat5 species

Fig. 8 – Values of propylene, ethylene and CO_x selectivities, as well as propylene yield for synthesized catalysts in this work at $500\text{ }^{\circ}\text{C}$, $C_3H_8/air = 0.6$ and feed flow rate of 90 mL min^{-1}

chosen according to Table 2) and those of different materials available in the open literature are presented in Table 3. These results further emphasized that the optimum synthesized catalyst in this research proved to be a rather good contender for the purpose at hand.

Table 3 – Comparison of vanadium catalysts for the ODHP reaction between the previous works and the best of the current study

Catalyst/oxidizing agent	T (°C)	C ₃ H ₈ conversion (%)	C ₃ H ₆ selectivity (%)	C ₃ H ₆ yield (%)	Reference
V ₂ O ₅ /O ₂	500	6.73	25.26	1.69	40
V ₂ O ₅ /N ₂ O	500	4.30	72.25	3.11	40
V ₂ O ₅ /Air	460	3.5	15.3	0.54	41
V-Al ₂ O ₃ /O ₂	700	22.8	25.0	5.7	42
CeO ₂	450	7.25	18.14	1.32	43
Mo-Ti/O ₂	500	22.2	11.3	2.51	44
Mo-Al/O ₂	500	19.1	37.6	7.18	44
V-Ti/O ₂	500	21.1	28.4	5.99	44
V-Al/O ₂	500	23.4	13.6	3.18	44
V-Ti-Al/O ₂	500	33.01	32.61	10.76	Present work

Conclusions

This research demonstrated facile V_2O_5 over synthesized nano- TiO_2 and $\gamma-Al_2O_3$ catalysts utilizing the hydrothermal technique. These materials were characterized by several methods, including BET-BJH, XRD, FTIR, H_2 -TPR and FESEM. Moreover, their performance was evaluated in a fixed bed reactor. It was indicated that, the prepared nano- TiO_2 catalysts were not only more stable, but also resulted in higher propylene yields when compared with that utilizing commercial TiO_2 as the support. In fact, propylene yields of about 10.76 % and propane conversions of 33.01 % were obtained over the Cat5 material. It was further determined that the oxidation and oxy-cracking reactions competed with the main ODHP reaction leading to the formation of ethylene and CO_x as the side products. Ultimately, this study has revealed that the vanadium pentoxide deposited over a hybrid of nanostructures of TiO_2 and $\gamma-Al_2O_3$ resulted in an attractive catalytic material applicable to the propane dehydrogenation reaction. Nonetheless, a thorough kinetic investigation of this synthesized material is underway to confirm this conclusion.

References

1. Barghi, B., Fattahi, M., Khorasheh, F., Kinetic modeling of propane dehydrogenation over an industrial catalyst in the presence of oxygenated compounds, *Reac. Kinet. Mech. Catal.* **107** (2012) 141.
doi: <http://dx.doi.org/10.1007/s11144-012-0455-z>
2. Fattahi, M., Kazemeini, M., Khorasheh, F., Rashidi, A. M., Vanadium pentoxide catalyst over carbon-based nanomaterials for the oxidative dehydrogenation of propane, *Ind. Eng. Chem. Res.* **52** (2013) 16128.
doi: <http://dx.doi.org/10.1021/ie4007358>
3. Cavani, F., Ballarini, N., Cericola, A., Oxidative dehydrogenation of ethane and propane: How far from commercial implementation?, *Catal. Today* **127** (2007) 113.
doi: <http://dx.doi.org/10.1016/j.cattod.2007.05.009>
4. Li, J.-H., Wang, C.-C., Huang, C.-J., Sun, Y.-F., Weng, W.-Z., Wan, H.-L., Mesoporous nickel oxides as effective catalysts for oxidative dehydrogenation of propane to propene, *Appl. Catal. A* **382** (2010) 99.
doi: <http://dx.doi.org/10.1016/j.apcata.2010.04.034>
5. Azzam, K. G., Jacobs, G., Shafer, W. D., Davis, B. H., Dehydrogenation of propane over Pt/KL catalyst: Investigating the role of L-zeolite structure on catalyst performance using isotope labeling, *Appl. Catal. A* **390** (2010) 264.
doi: <http://dx.doi.org/10.1016/j.apcata.2010.10.022>
6. Michorczyk, P., Ogonowski, J., Kustrowski, P., Chmielarz, L., Chromium oxide supported on MCM-41 as a highly active and selective catalyst for dehydrogenation of propane with CO_2 , *Appl. Catal. A* **349** (2008) 62.
doi: <http://dx.doi.org/10.1016/j.apcata.2008.07.008>
7. Chen, M., Xu, J., Liu, Y.-M., Cao, Y., He, H.-Y., Zhuang, J.-H., Supported indium oxide as novel efficient catalysts for dehydrogenation of propane with carbon dioxide, *Appl. Catal. A* **377** (2010) 35.
doi: <http://dx.doi.org/10.1016/j.apcata.2010.01.011>
8. Kotanjac, Z. S., van Sint Annaland, M., Kuipers, J. A. M., A packed bed membrane reactor for the oxidative dehydrogenation of propane on a Ga_2O_3/MoO_3 based catalyst, *Chem. Eng. Sci.* **65** (2010) 441.
doi: <http://dx.doi.org/10.1016/j.ces.2009.04.015>
9. Boucetta, C., Kacimi, M., Ensuque, A., Piquemal, J.-Y., Bazon-Verduraz, F., Ziyad, M., Oxidative dehydrogenation of propane over chromium-loaded calcium-hydroxyapatite, *Appl. Catal. A* **356** (2009) 201.
doi: <http://dx.doi.org/10.1016/j.apcata.2009.01.005>
10. Kung, H. H., Oxidative dehydrogenation of light (C_2 to C_4) alkanes, *Adv. Catal.* **40** (1994) 1.
doi: [http://dx.doi.org/10.1016/S0360-0564\(08\)60655-0](http://dx.doi.org/10.1016/S0360-0564(08)60655-0)
11. Mamedov, E. A., Cortes Corberan, V., Oxidative dehydrogenation of lower alkanes on vanadium oxide-based catalysts. The present state of the art and outlooks, *Appl. Catal. A* **127** (1995) 1.
doi: [http://dx.doi.org/10.1016/0926-860X\(95\)00056-9](http://dx.doi.org/10.1016/0926-860X(95)00056-9)
12. Blasco, T., Lopez-Nieto, J. M., Oxidative dehydrogenation of short chain alkanes on supported vanadium oxide catalysts, *Appl. Catal. A* **157** (1997) 117.
doi: [http://dx.doi.org/10.1016/S0926-860X\(97\)00029-X](http://dx.doi.org/10.1016/S0926-860X(97)00029-X)
13. Albonetti, S., Cavani, F., Trifiro, F., Key aspects of catalyst design for the selective oxidation of paraffins, *Catal. Rev.: Sci. Eng.* **38** (1996) 413.
doi: <http://dx.doi.org/10.1080/01614949608006463>
14. Le Bars, J., Auroux, A., Forissier, M., Vedrine, J. C., Active sites of $V_2O_5/\gamma-Al_2O_3$ catalysts in the oxidative dehydrogenation of ethane, *J. Catal.* **162** (1996) 250.
doi: <http://dx.doi.org/10.1006/jcat.1996.0282>
15. Grzybowska-Swierkosz, B., Effect of additives on the physicochemical and catalytic properties of oxide catalysts in selective oxidation reactions, *Top. Catal.* **21** (2002) 35.
doi: <http://dx.doi.org/10.1023/A:1020547830167>
16. Kondratenko, E. V., Baerns, M., Catalytic oxidative dehydrogenation of propane in the presence of O_2 and N_2O -the role of vanadia distribution and oxidant activation, *Appl. Catal. A* **222** (2001) 133.
doi: [http://dx.doi.org/10.1016/S0926-860X\(01\)00836-5](http://dx.doi.org/10.1016/S0926-860X(01)00836-5)
17. Leveles, L., Seshan, K., Lercher, J. A., Lefferts, L., Oxidative conversion of propane over lithium-promoted magnesia catalyst: I. Kinetics and mechanism, *J. Catal.* **218** (2003) 296.
doi: [http://dx.doi.org/10.1016/S0021-9517\(03\)00112-X](http://dx.doi.org/10.1016/S0021-9517(03)00112-X)
18. Heracleous, E., Machli, M., Lemonidou, A. A., Vasalos, I. A., Oxidative dehydrogenation of ethane and propane over vanadia and molybdena supported catalysts, *J. Mol. Catal. A: Chem.* **232** (2005) 29.
doi: <http://dx.doi.org/10.1016/j.molcata.2005.01.027>
19. Argyle, M. D., Chen, K., Bell, A. T., Iglesia, E., Effect of catalyst structure on oxidative dehydrogenation of ethane and propane on alumina-supported vanadia, *J. Catal.* **208** (2002) 139.
doi: <http://dx.doi.org/10.1006/jcat.2002.3570>
20. Stelzer, J. B., Caro, J., Fait, M., Oxidative dehydrogenation of propane on TiO_2 supported antimony oxide/vanadia catalysts, *Catal. Commun.* **6** (2005) 1.
doi: <http://dx.doi.org/10.1016/j.catcom.2004.10.001>
21. Lemonidou, A. A., Nalbandian, L., Vasalos, I. A., Oxidative dehydrogenation of propane over vanadium oxide based catalysts: Effect of support and alkali promoter, *Catal. Today* **61** (2000) 333.
doi: [http://dx.doi.org/10.1016/S0920-5861\(00\)00393-X](http://dx.doi.org/10.1016/S0920-5861(00)00393-X)
22. Alexopoulos, K., Reyniers, M.-F., Marin, G. B., Reaction path analysis of propane selective oxidation over V_2O_5 and V_2O_5/TiO_2 , *J. Catal.* **289** (2012) 127.

- doi: <http://dx.doi.org/10.1016/j.jcat.2012.01.019>
23. Zhu, Q., Takiguchi, M., Setoyama, T., Yokoi, T., Kondo, J. N., Tatsumi, T., Oxidative dehydrogenation of propane with CO₂ over Cr/H[B]MFI catalysts, *Catal. Lett.* **141** (2011) 670. doi: <http://dx.doi.org/10.1007/s10562-011-0566-6>
24. Singh, R. P., Bañares, M. A., Deo, G., Effect of phosphorous modifier on V₂O₅/TiO₂ catalyst: ODH of propane, *J. Catal.* **233** (2005) 388. doi: <http://dx.doi.org/10.1016/j.jcat.2005.05.010>
25. Cheng, L., Ferguson, G. A., Zygmunt, S. A., Curtiss, L. A., Structure-activity relationships for propane oxidative dehydrogenation by anatase-supported vanadium oxide monomers and dimmers, *J. Catal.* **302** (2013) 31. doi: <http://dx.doi.org/10.1016/j.jcat.2013.02.012>
26. Castro, A. J. R., Marques, S. P. D., Soares, J. M., Filho, J. M., Saraiva, G. D., Oliveira, A. C., Nanosized aluminum derived oxides catalysts prepared with different methods for styrene production, *Chem. Eng. J.* **209** (2012) 345. doi: <http://dx.doi.org/10.1016/j.cej.2012.07.094>
27. Shee, D., Deo, G., Hirt, A. M., Characterization and reactivity of sol-gel synthesized TiO₂-Al₂O₃ supported vanadium oxide catalysts, *J. Catal.* **273** (2010) 221. doi: <http://dx.doi.org/10.1016/j.jcat.2010.05.017>
28. Lofberg, A., Giornelli, T., Paul, S., Bordes-Richard, E., Catalytic coatings for structured supports and reactors: VO_x/TiO₂ catalyst coated on stainless steel in the oxidative dehydrogenation of propane, *Appl. Catal. A* **391** (2011) 43. doi: <http://dx.doi.org/10.1016/j.apcata.2010.09.002>
29. Arena, F., Frusteri, F., Parmaliana, A., Martra, G., Coluccia, S., Oxidative dehydrogenation of propane on supported V₂O₅ catalysts. The role of redox and acid-base properties, *Stud. Surf. Sci. Catal.* **119** (1998) 665. doi: [http://dx.doi.org/10.1016/S0167-2991\(98\)80508-9](http://dx.doi.org/10.1016/S0167-2991(98)80508-9)
30. Martin-Aranda, R. M., Portela, M. F., Madeira, L. M., Freire, F., Oliveira, M., Effect of alkali metal promoters on nickel molybdate catalysts and its relevance to the selective oxidation of butane, *Appl. Catal. A* **27** (1995) 201. doi: [http://dx.doi.org/10.1016/0926-860X\(95\)00037-2](http://dx.doi.org/10.1016/0926-860X(95)00037-2)
31. Zima, T. M., Baklanova, N. I., Utkin, A. V., Hydrothermal synthesis of a nanostructured TiO₂-based material in the presence of chitosan, *Inorg. Mater.* **48** (2012) 821. doi: <http://dx.doi.org/10.1134/S0020168512080171>
32. Bezrodna, T., Puchkovska, G., Shymanovska, V., Baran, J., Ratajczak, H., IR-analysis of H-bonded H₂O on the pure TiO₂ surface, *J. Mol. Struct.* **700** (2004) 175. doi: <http://dx.doi.org/10.1016/j.molstruc.2003.12.057>
33. Vuurman, M. A., Stufkens, D. J., Oskam, A., Deo, G., Wachs, I. E., Combined Raman and IR study of MO_x-V₂O₅/Al₂O₃ (MO_x = MoO₃, WO₃, NiO, CoO) catalysts under dehydrated conditions, *J. Chem. Soc. Faraday Trans.* **92** (1996) 3259. doi: <http://dx.doi.org/10.1039/ft9969203259>
34. Vuurman, M. A., Wachs, I. E., Stufkens, D. J., Oskam, A., Characterization of chromium oxide supported on Al₂O₃, ZrO₂, TiO₂, and SiO₂ under dehydrated conditions, *J. Mol. Catal.* **80** (1993) 209. doi: [http://dx.doi.org/10.1016/0304-5102\(93\)85079-9](http://dx.doi.org/10.1016/0304-5102(93)85079-9)
35. Courtine, P., Bordes, E., Mode of arrangement of components in mixed vanadia catalyst and its bearing for oxidation catalysis, *Appl. Catal., A* **157** (1997) 45. doi: [http://dx.doi.org/10.1016/S0926-860X\(97\)00020-3](http://dx.doi.org/10.1016/S0926-860X(97)00020-3)
36. Abello, M. C., Gomez, M. F., Ferretti, O., Mo/γ-Al₂O₃ catalysts for the oxidative dehydrogenation of propane. Effect of Mo loading, *Appl. Catal. A* **207** (2001) 421. doi: [http://dx.doi.org/10.1016/S0926-860X\(00\)00680-3](http://dx.doi.org/10.1016/S0926-860X(00)00680-3)
37. Went, G. T., Oyama, S. T., Bell, A. T., Laser Raman spectroscopy of supported vanadium oxide catalysts, *J. Phys. Chem.* **94** (1990) 4240. doi: <http://dx.doi.org/10.1021/j100373a067>
38. Rao, T. V. M., Deo, G., Ethane and propane oxidation over supported V₂O₅/TiO₂ catalysts: Analysis of kinetic parameters, *Ind. Eng. Chem. Res.* **46** (2007) 70. doi: <http://dx.doi.org/10.1021/ie060715w>
39. Rao, T. V. M., Deo, G., Kinetic parameter analysis for propane ODH: V₂O₅/Al₂O₃ and MoO₃/Al₂O₃ catalysts, *AIChE J.* **53** (2007) 1538. doi: <http://dx.doi.org/10.1002/aic.11176>
40. Kondratenko, E. V., Ovsitser, O., Radnik, J., Schneider, M., Kraehnert, R., Dingerdissen, U., Influence of reaction conditions on catalyst composition and selective/non-selective reaction pathways of the ODP reaction over V₂O₅, VO₂ and V₂O₃ with O₂ and N₂O, *Appl. Catal. A* **319** (2007) 98. doi: <http://dx.doi.org/10.1016/j.apcata.2006.11.021>
41. Balderas-Tapia, L., Hernández-Pérez, I., Schacht, P., Córdova, I. R., Aguilar-Ríos, G. G., Influence of reducibility of vanadium-magnesium mixed oxides on the oxidative dehydrogenation of propane, *Catal. Today* **107-108** (2005) 371. doi: <http://dx.doi.org/10.1016/j.cattod.2005.07.025>
42. Clark, P. D., Dowling, N. I., Long, X., Li, Y., Oxidative dehydrogenation of propane to propene in the presence of H₂S at short contact times, *J. Sulf. Chem.* **25** (2004) 381. doi: <http://dx.doi.org/10.1080/17415990412331327909>
43. Sugiyama, S., Iizuka, Y., Nitta, E., Hayashi, H., Moffat, J. B., Role of tetrachloromethane as a gas-phase additive in the oxidative dehydrogenation of propane over cerium oxide, *J. Catal.* **189** (2000) 233. doi: <http://dx.doi.org/10.1006/jcat.1999.2700>
44. Heracleous, E., Machli, M., Lemonidou, A. A., Vasalos, I. A., Oxidative dehydrogenation of ethane and propane over vanadia and molybdena supported catalysts, *J. Mol. Catal. A: Chem.* **232** (2005) 29. doi: <http://dx.doi.org/10.1016/j.molcata.2005.01.027>